



City Research Online

City, University of London Institutional Repository

Citation: Arrell, K., Wise, S., Wood, J. & Donoghue, D. (2008). Spectral filtering as a method of visualising and removing striped artefacts in digital elevation data. *Earth Surface Processes and Landforms*, 33(6), pp. 943-961. doi: 10.1002/esp.1597

This is the unspecified version of the paper.

This version of the publication may differ from the final published version.

Permanent repository link: <https://openaccess.city.ac.uk/id/eprint/533/>

Link to published version: <https://doi.org/10.1002/esp.1597>

Copyright: City Research Online aims to make research outputs of City, University of London available to a wider audience. Copyright and Moral Rights remain with the author(s) and/or copyright holders. URLs from City Research Online may be freely distributed and linked to.

Reuse: Copies of full items can be used for personal research or study, educational, or not-for-profit purposes without prior permission or charge. Provided that the authors, title and full bibliographic details are credited, a hyperlink and/or URL is given for the original metadata page and the content is not changed in any way.

City Research Online:

<http://openaccess.city.ac.uk/>

publications@city.ac.uk

SPECTRAL FILTERING AS A METHOD OF VISUALISING AND REMOVING STRIPED ARTEFACTS IN DIGITAL ELEVATION DATA

Katherine Arrell^{1*}, Steve Wise², Jo Wood³ and Danny Donoghue⁴

¹School of Geography, Earth and Biosphere Institute, University of Leeds, LS2 9JT, UK, ²Department of Geography, Sheffield University, Sheffield, S10 2TN, ³The giCentre, City University London, EC1V OHB, ⁴ Department of Geography, Durham University, Durham, DH1 3LE.

*Corresponding author: k.arrell@leeds.ac.uk

Abstract

Spectral filtering was compared with traditional mean spatial filters to assess their ability to identify and remove striped artefacts in digital elevation data. The techniques were applied to two datasets: a 100 m contour derived digital elevation model (DEM) of southern Norway and a 2 m LiDAR DSM of the Lake District, UK. Both datasets contained diagonal data artefacts that were found to propagate into subsequent terrain analysis. Spectral filtering used fast Fourier transformation (FFT) frequency data to identify these data artefacts in both datasets. These were removed from the data by applying a cut filter, prior to the inverse transform. Spectral filtering showed considerable advantages over mean spatial filters, when both the absolute and spatial distribution of elevation changes made were examined. Elevation changes from the spectral filtering were restricted to frequencies removed by the cut filter, were small in magnitude and consequently avoided any global smoothing. Spectral filtering was found to avoid the smoothing of kernel based data editing, and provided a more informative measure of data artefacts present in the FFT frequency domain. Artefacts were found to be heterogeneous through the surfaces, a result of their strong correlations with spatially autocorrelated variables: landcover and landsurface geometry. Spectral filtering performed better on the 100 m DEM, where signal and artefact were clearly distinguishable in the frequency data. Spectrally filtered digital elevation datasets were found to provide a superior and more precise representation of the landsurface and be a more appropriate dataset for any subsequent geomorphological applications.

Keywords: digital elevation model; terrain analysis; geographical information science

1. Introduction

Since the nature of the terrain surface is of such central importance in geomorphology, it is hardly surprising that digital elevation models (DEMs) are widely used within the discipline. The existence of digital representations of the terrain surface, and software to manipulate them, has given a new impetus to the field of geomorphometry (Pike, 2000; Hengl and Evans, 2007) and led to the development of new approaches to the identification of fundamental landscape structures such as ridges and valleys (Wood, 1996; Dragut and Blashke, 2007) and the identification of individual landforms (Miliaresis, 2006; Prima et al., 2006; Arrell et al., 2007). Over

short timescales, the terrain surface is a key factor in many environmental processes, having a major effect on key climatic parameters such as temperature and precipitation, and controlling the rate and spatial pattern of processes of weathering, erosion and deposition across a surface (Moore et al., 1991; Wilson and Gallant, 2000; Arrell, 2005). Over long timescales these processes shape the terrain, and researchers are increasingly using analysis of terrain characteristics to help infer long-term denudational histories of regions (Bishop et al., 2002; Brocklehurst and Whipple, 2006).

Early DEMs tended to be derived from contours on topographic maps or from aerial photography. These typically varied in resolution from 1 km global DEMs, such as GTOPO30 (http://edc.usgs.gov/products/elevation/gtopo30_gtopo30.html) to 10–50 m DEMs produced by national mapping agencies such as the Ordnance Survey in Great Britain (www.ordnancesurvey.co.uk). Developments in techniques for capturing height data from Earth observation platforms have led to three major developments. Height data can be sampled uniformly across large areas. The best example of this is the near global coverage (56° S to 60° N) of NASA's Shuttle Radar Topography Mission (SRTM; <http://srtm.usgs.gov/>), which provides 3 arc-second resolution (~90 m at the Equator) data produced using synthetic aperture radar (SAR) interferometry. Very high-resolution data of the order of 1 m can be produced, especially using light detecting and ranging (LiDAR) technology (Ritchie, 1996). Information is now available on the height of the upper surface (often referred to as a digital surface model – DSM), which in many cases is not the terrain but vegetation and buildings that rest upon it. For some applications, this represents an element of noise, which must be removed to reveal the underlying terrain surface, but for others it provides useful information on the true roughness of the surface and on the nature and distribution of vegetation.

Given the widespread use of DEMs, it is important to have an understanding of their accuracy. This is partly an issue of scale, and the degree to which a DEM represents the landscape. Nyquist sampling theory suggests that a DEM cannot represent anything smaller than twice the pixel spacing, so that whereas a 2 m LiDAR DEM might readily represent hillslope gullies, a 1 km DEM only represents major ridges and valleys. However, DEMs at all scales contain error from a variety of sources (Fisher and Tate, 2006), and this error can propagate to any analyses undertaken with the DEM.

The study of error and its propagation has become an important area in geographical information science (GIS), nowhere more so than in the case of DEMs (Temme et al., 2007). The large body of work on DEM error is a reflection of the widespread use of these datasets in a range of applications, the increasing confidence we must place in the results of these applications and the increasing range of digital elevation data products available.

Elevation data differ from most other environmental data in that individual data values are almost never sufficient in themselves to answer any meaningful query (Wise, 2002). This is because these data values are simply samples from a surface of continuous variation, and it is this surface that is commonly of interest. Thus, given a sample of elevation points, or a series of contours across the surface, it is not necessarily possible to directly answer a query relating to surface elevation, such as

‘what is the elevation at this point?’ An answer requires a model of the surface between sampled points. Such a model has to be produced by interpolation between sampled values, and since interpolation is an estimation procedure, the surface will contain a degree of error. This means that in addition to the measurement errors inherent in all data, DEMs also contain interpolation errors.

The two most common models of surfaces, model the area between sampled values differently. In a triangulated irregular network (TIN), original data points are connected by a series of triangles. Interpolation thus takes place when it is necessary to derive values for points inside these triangles. More common, gridded DEMs are created by interpolating values onto an array of regularly spaced points. The regularity of the grid inherently contains information about the topology of the points, and it is a simple matter to derive algorithms that calculate values for a surface in between the gridded DEM points (Wilson and Gallant, 2000). A gridded DEM usually contains interpolation error, unless the points have been measured on a regular grid, and further interpolation error can arise when values are estimated from the grid (e.g. elevation at a non-grid point).

This paper is concerned with striped errors within gridded DEMs, these are common in photogrammetrically derived DEMs (Albani and Klinkenberg, 2003) and can be introduced through data resampling. As we will be concerned exclusively with gridded DEMs, for simplicity we will use the term DEM to refer to this data structure. Despite the merits of TINs for modelling a surface explicitly, and having the potential to directly represent key landscape elements such as peaks, ridges and valleys (Peucker et al., 1978; Kumler, 1994), gridded DEMs are by far the most commonly used format for elevation data, because of their processing simplicity, the wide availability of raster software and their easy transfer between systems.

2. Modelling DEM error

A large body of literature exists on error in DEMs and recent work by Fisher and Tate (2006) provides an excellent review. Error in DEMs is usually categorized into three types: blunders, random and systematic error (Cooper, 1998; Fisher and Tate, 2006). Blunders are gross errors, often caused by operator error or machine malfunction, and are relatively easy to detect. Much research on errors and error propagation focuses on random error, because there is the potential to model this theoretically. The simplest assumption is that errors in a DEM are random and thus follow a normal distribution. Comparison between values in the DEM with a sample of values from a more accurate source provide an estimate of this error, most commonly as the root mean square error (RMSE)

$$RMSE = \sqrt{\frac{\sum (Z_{DEM} - Z_{ref})^2}{n}}$$

where Z_{DEM} is the DEM model elevation, Z_{ref} is the reference or validation elevation and n is the number of samples. Normally this value is a global aspatial measure, derived from only a sample of data points. Although this measure provides information relating to the average error, increasing applications of digital datasets and demands on the confidence we place on their resultant outputs necessarily require

more informative error measures. Research has attempted to study potential effects of error on results produced from DEMs by applying random error to a DEM and using Monte Carlo simulation to look at the effect this has on DEM results (Hunter and Goodchild, 1997; Fisher, 1998). It is recognized of course that error in DEMs is not in fact completely random but contains a systematic element. Thapa and Bossler (1992, p. 836) define systematic errors as result of a ‘deterministic system which if known may be represented by some functional system’. These systematic errors can arise in a number of ways.

Error originating from interpolation, an inherently spatial process, has been built into error modelling effects by including a spatial autocorrelation element into the modelled error field (Hunter and Goodchild, 1997; Fisher, 1998). Yet, still some systematic errors in DEMs are not well modelled by a spatial autocorrelation function applied globally to the whole surface. Two well-known examples arise with interpolation from contour data. The first is a tendency for grid points near contours to take on a value very close to or the same as the contour value (Wood and Fisher, 1993; Wise, 1998; Fisher and Tate, 2006) (an effect exacerbated by converting elevation values to integer). The second, a manifestation of the first, is an abrupt change in estimated elevation midway between successive contours. Both systematic interpolation errors produce a set of artefacts in the DEM which mirror the original contour lines, and are hence strongly related to terrain shape. Spatial autocorrelation is consequently present in these errors, but is strongly anisotropic, operating parallel to the original contours. This potentially could be modelled by a spatial autocorrelation function, which would have to take into account the local slope direction. We are not currently aware whether this has been attempted. Another well-known artefact which might present more of a challenge for formal statistical modelling are triangular facets within a gridded DEM. These occur across valleys and ridges when a Delaunay triangulation is applied to interpolate between digitized contour data. This arises because in these locations three points on the same contour can form the corners of a Delaunay triangle, producing an erroneous flat surface.

Systematic error is also common as striping in DEMs, this can originate from resampling data from a geographical to a UTM projection or introduced as an artefact of data collection or during the processing of photogrammetrically derived DEMs (Kok and Rangayyan, 1987). Data stripes are common in a range of DEM products, most commonly noted in Level 1 USGS DEMs (defined as those derived from photogrammetric methods) introduced through manual profiling or scanning methods (Brunson and Olsen, 1978; Hassan, 1988; Klinkenberg and Goodchild, 1992; Brown and Bara, 1994; Garbrecht and Starks, 1995; Oimoen, 2000), similarly stripes are found in terrain resource information management (TRIM) data as a result of oversampling along collection lines (Albani and Klinkenberg, 2003) and are also present in Shuttle Radar Topography Mission (SRTM) data as result of uncompensated mast motion error (Walker et al., 2007). The striped artefacts present within these datasets rapidly propagate through subsequent analysis (Holmes et al., 2000).

Error and artefacts are also problematic in LiDAR data (Sithole and Vosselman, 2003, 2004) used to create DSMs. Within a DSM, elevation values recorded not only represent a terrain surface, but could also include any above-surface features (Chen, 2007). Artefacts and error in LiDAR derived DSMs are introduced through LiDAR

system settings, aircraft pitch calibration, interpolation, horizontal displacement error and surveyor error. Discussion of the characteristics of these errors and artefacts has found them to be spatially organized, relating to landcover patterns and topographic characteristics, predominantly slope (Su and Bork, 2006; Hodgson and Bresnahan, 2004). The need for improved filtering techniques of LiDAR data was expressed by Sithole and Vosselman (2003, 2004) and also noted by Flood (2001), who suggested that data filtering and point removal consumed 60–80% of LiDAR data processing time.

Besides identifying and modelling errors in DEMs, work has also concentrated on correcting errors to improve DEM quality. Error is normally defined to be the difference between a model value and the true value (Fisher and Tate, 2006). Standard measures of DEM error are described in terms of the metric accuracy of elevation values. However, a narrow focus on metric accuracy is not necessarily a good approach to error detection and correction in DEMs, as many applications of DEMs do not rely on accurate elevation values but do need a faithful representation of surface shape. For example, in generating a drainage network using standard flow direction methods (e.g. Jenson and Domingue, 1991), it would not matter if elevation values were consistently 5 m too high, so long as the shape of slopes and valleys was accurately represented. This is where the nature of artefacts becomes important. Artefacts may represent relatively small errors in absolute elevation but if they are systematic, they can produce systematic errors in the results produced from DEMs. For example, flat triangles in a DEM derived from triangulated contours will produce errors in a derived drainage network (Wise, 2000). Errors that are spatially autocorrelated along DEM grid rows or columns can produce unrealistic stripes in the computed slope, aspect or curvature layers.

3. Case study DEMs

Performance of a spectral filtering and spatial mean filters to identify and remove DEM artefacts was compared on two contrasting scale DEMs, i) a 100 m DEM of the central Jotunheimen, Norway; and ii) a 2m DEM of Loughrigg Fell, Lake District, UK.

Jotunheimen

The Jotunheimen region of southern Norway represents a glaciated landscape of high relief with major interconnecting valley systems (Figure 1). The DEM was created by Statens kartverk, who applied a nearest neighbour inverse distance weighted algorithm to interpolate the DEM from digitized contour lines. Two interrelated error components were found to be present in the elevation surface: contour altitude spikes due to the oversampling of contour altitudes in the interpolation process (Figure 2a) and two persistent diagonal trends in the data (Figure 1). Although the source of these is not confirmed, it is suggested by the authors that it is either a result of a non-linear transformation from geographical coordinates to projected UTM or simply a result of the nearest neighbour interpolation that treated diagonal and orthogonal components differently.

Propagation of these artefacts, predominantly through surface derivatives, is particularly apparent in the DEM surface gradient data. Such data are commonly used

in terrain and hydrological modelling applications, results from which can be biased by the strong spatial pattern of the artefacts. Although in part a result of inadequate flow algorithms and data resolution, derived flow accumulation data for this DEM showed uncharacteristic channel networks (Figure 3a), with parallel channels and linear flow segments.

As previously discussed, systematic errors, which are uniform across a surface, tend to be easy to resolve, where altitudinal adjustments and error bars can be applied with confidence. However, most known error in terrain surfaces is topographically organized (Wood, 1996). This organization is apparent within our DEM where the dominance (magnitude) of diagonal striping in derivative surfaces is greater in areas of moderate terrain than in smoother areas.

Loughrigg Fell

The LiDAR derived DSM of the western slopes of Loughrigg Fell, Lake District, UK, again represents a largely glacial topography, but at much higher resolution than the Norwegian DEM (Figure 4). The DSM contains surface vegetation features.

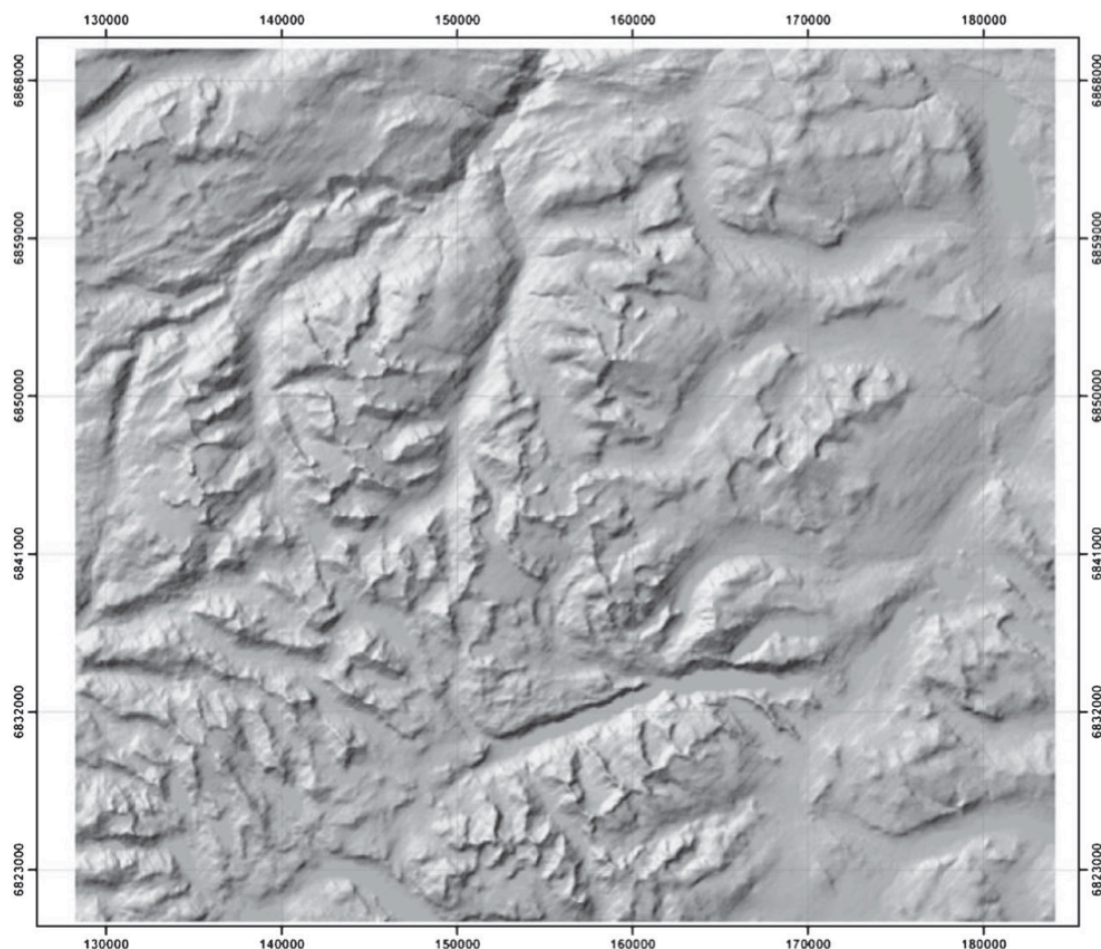


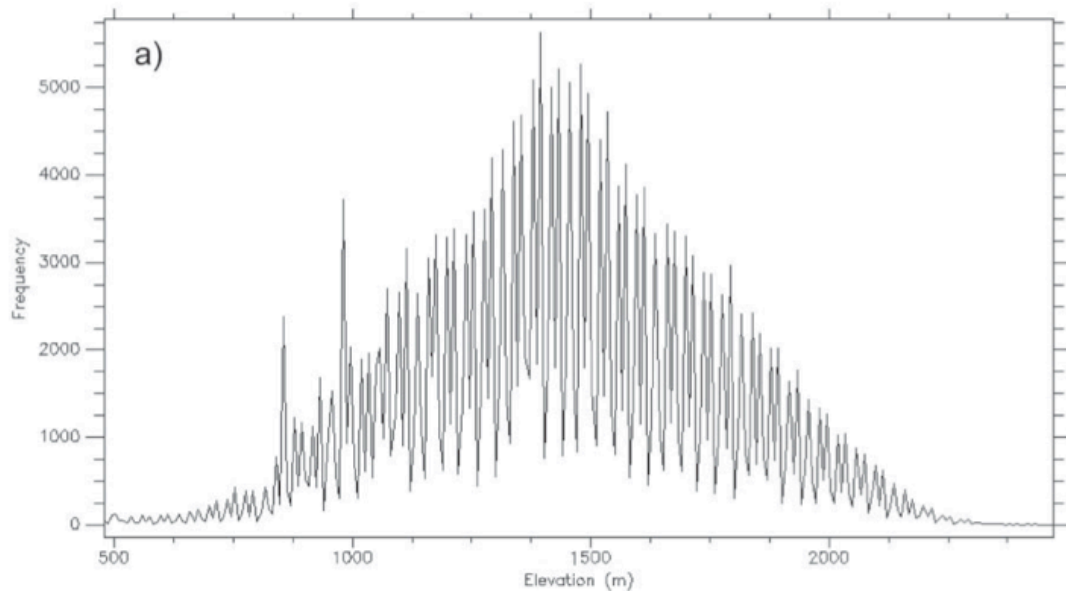
Figure 1: Hillshade image of the Norwegian study area DEM of the Jotunheimen showing the dominant artefact banding, image is illuminated from the northwest.

The predominant characteristic of the artefacts within the Loughrigg DSM is again a diagonal banding here in two dominant directions ($\sim 75^\circ$ and 143°), an artefact from aircraft pitch calibration (Figure 4). Less apparent in the elevation frequency

histogram, the banding propagates into higher order elevation derivatives, namely surface gradient, plan and profile curvature. Flow direction data, a prerequisite for most flow accumulation algorithms, is particularly responsive to the banding, introducing a directional bias into subsequent flow routing data. As was seen in the Norwegian DEM, the magnitude of the banding in the Loughrigg DSM is not uniform across the surface.

4. Spectral Filtering

Rayner (1971, p. 72) considered that any variable or phenomenon that can be ordered according to increasing or decreasing wavelengths, should be viewed and treated as a spectrum, which he defined as ‘the scale breakdown of a phenomenon in space or time’. Spectral analysis is the mathematical characterization of differing wavelength components. Fast Fourier transformation (FFT) is an example of spectral analysis and quantifies the amplitude and phase angles of sinusoidal curves, which are fitted by least squares, to data that may be in one, two or n dimensions.



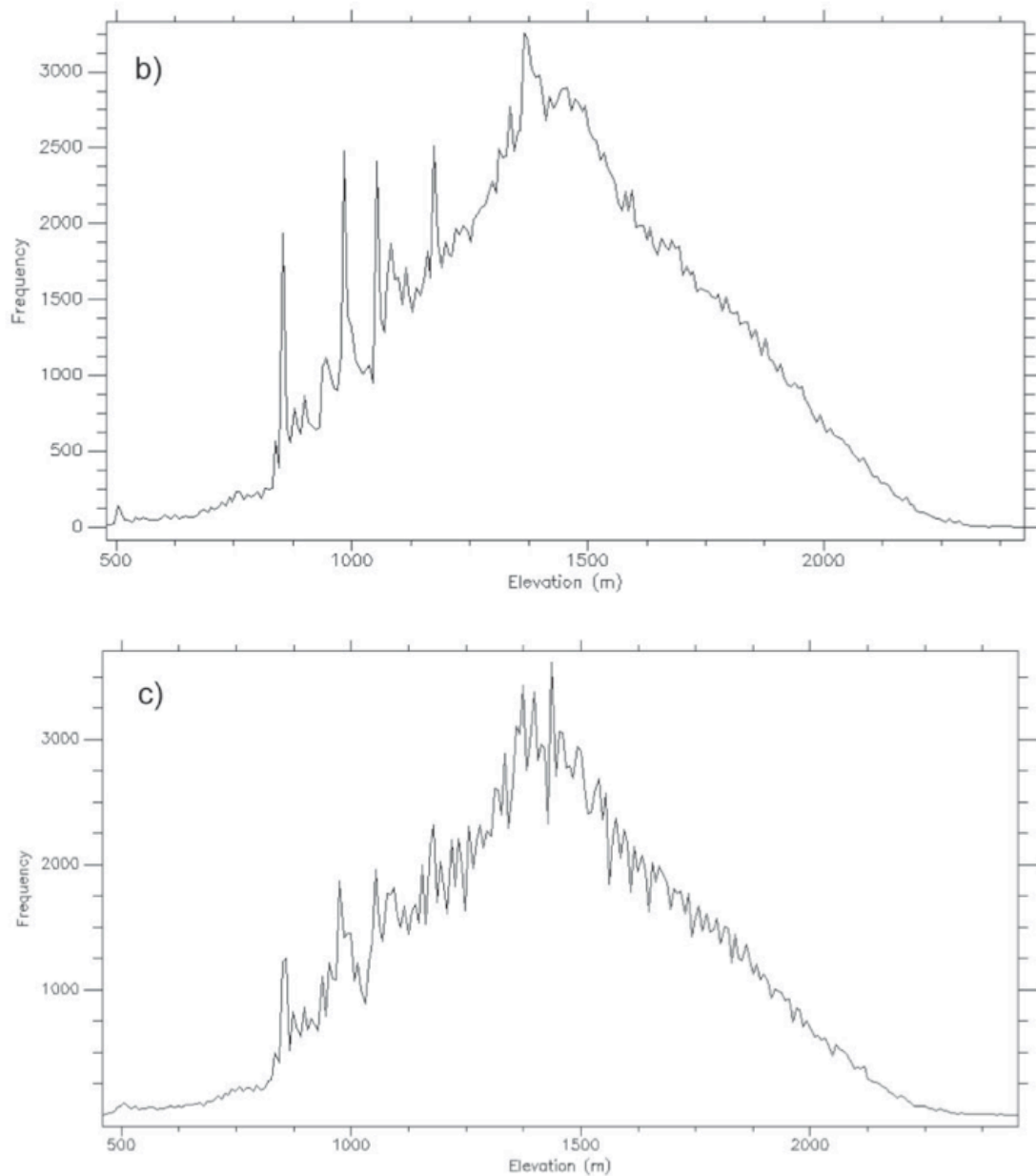


Figure 2. Frequency distributions of elevations within a) the original 100 m digital elevation model (DEM), b) the 3×3 smoothed DEM and c) the spectrally filtered DEM of Norway all highlighting data spikes. The original DEM a) highlights the magnitude of the data spikes, the 3×3 smoothed data b) shows a much smoothed data distribution with data spikes predominantly removed and the spectrally filtered dataset c) shows a more complex frequency distribution than found in the equivalent 3×3 spatial mean filtered dataset.

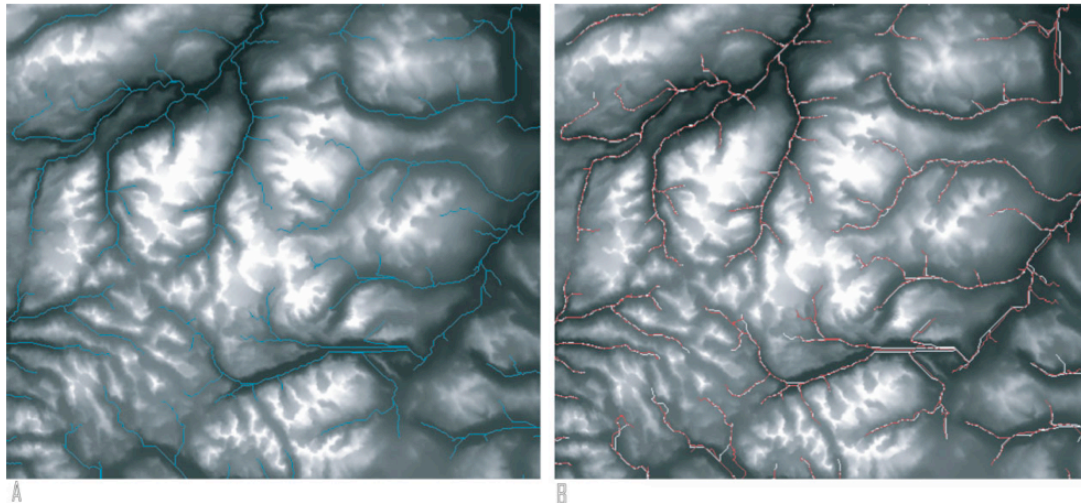


Figure 3. Flow accumulation networks draped on the original DEM a) original DEM network b) filtered DEM networks, white lines represent network from the 3*3 mean filter and red lines represent the network from the FFT data, note linear and parallel flow structures in both the original and 3*3 flow data.

Rayner (1971) applied Fourier transforms to environmental data performing a two-dimensional transform to digital maps of two drainage networks. The Fourier transform frequency spectra were found to be an effective mechanism for identifying and quantifying spacing and alignment of drainage networks, extracting data that was not otherwise easily retrievable. More recently Jordan and Schott (2005) used an FFT to identify tectonic faults, which were distinguish- able by their persistent orientation.

The application of Fourier transforms to identify and remove interference or artefact patterns is not new, early work performed by Dobrin et al. (1965) demonstrated its use in processing seismic data. More recently Liu and Jezek (1999) applied Fourier transforms and directional variograms to investigate the spatial structure and spatial autocorrelation of error within a DEM. They used Fourier transforms to investigate DEM error, however, in their work they made use of a higher resolution DEM of the same area, which allowed them to investigate the spatial structure of the error based on a large sample of error measurements. In the present study, spectral analysis was applied directly to the DEM to try and distinguish the ‘noise’ produced by the striped artefacts from the landscape signal.

For simplicity we conceptualize spectral filtering to be comprised of three stages. The initial stage of the process, ‘the FFT forward transform’, converts the data from the spatial domain into the frequency domain.

This frequency dataset represents the frequency of every data value in the input spatial dataset, displaying both the horizontal and vertical spatial frequency components. The average elevation (the zero frequency component or DC term) is shown in the centre of the FFT image, data values at an increasing radial distance from this central value represent increasing spatial frequency components. This frequency or magnitude image contains information about the geometric structure of the spatial domain image, where brightness (digital number) represents the amplitude of the frequency component and direction of any frequency component to the DC term represents the direction of the frequency components in the DEM. When applied to gridded continuous data these FFT data can show strong crosshairs within the frequency data,

representing high frequency variations between adjacent pixels and at the start and end of rows and columns. Interpretation of the FFT frequency data provides information about the structure and magnitude of the frequency organized components of the input data, here predominantly digital elevation data and their artefacts.

Following Rayner (1971) and Liu and Jezek (1999) the mean of both the DEM and DSM were removed prior to performing the transform in order to minimize leakage and interference between frequency bands, which can cause problems in resolving the frequency data (Liu and Jezek, 1999). The mean was replaced after the inverse transform had been applied. Further pre-filtering or windowing, commonly applied in order to amplify frequencies within the input data, was not used as aliasing did not appear to inhibit results, although this is an area that has been identified for future study.

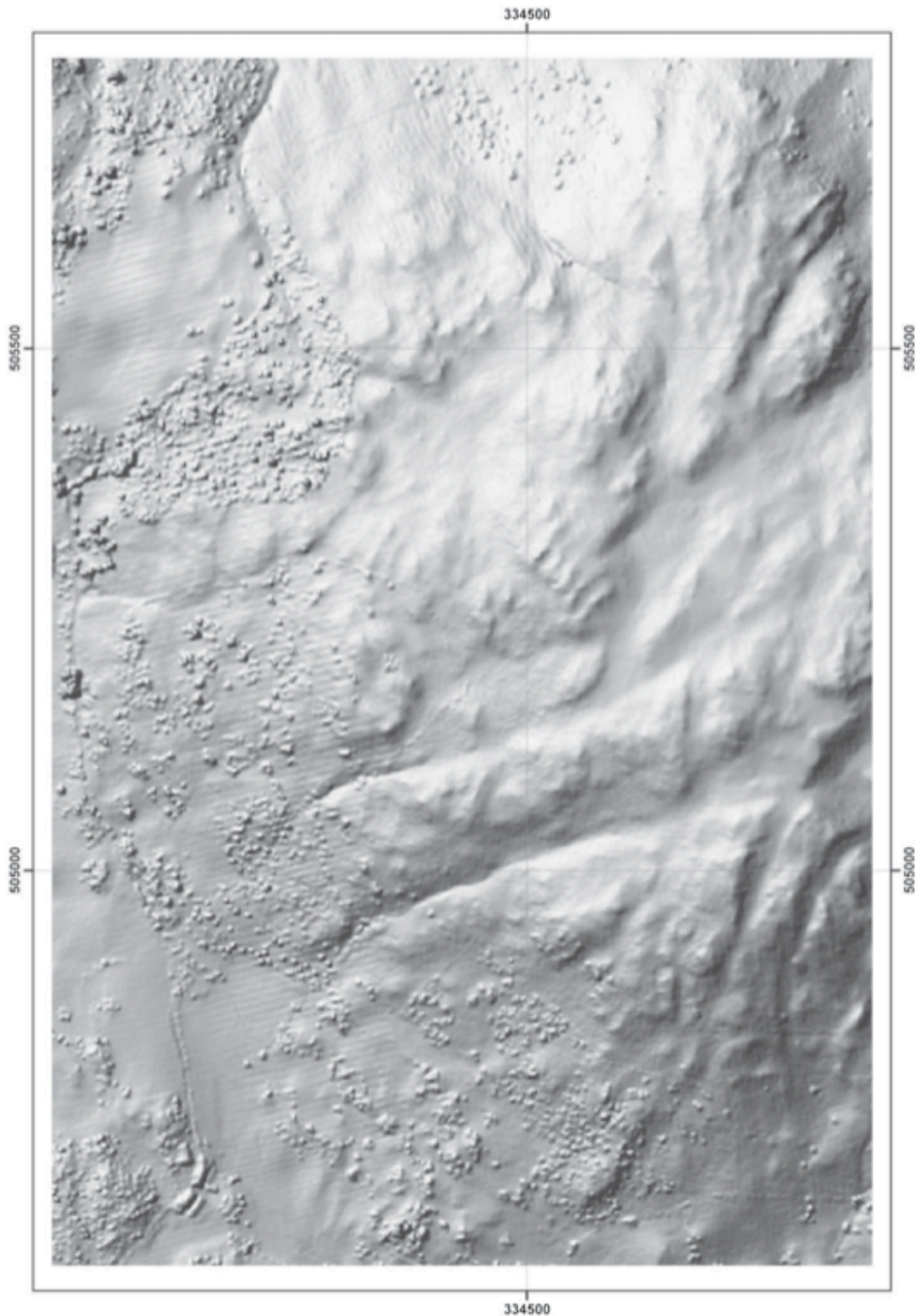


Figure 4. Hillshade image of the light detecting and ranging (LiDAR) 2 m digital surface model (DSM) of Loughrigg Fell, English Lake District, highlighting the artefact banding. The image is illuminated from the northwest. LiDAR data copyright Environment Agency Science Enterprise Centre.

An FFT was applied to each of the study area digital elevation datasets and the FFT frequency domain data was used to discriminate between signal and artefact. Artefact frequency components can be identified within FFT frequency data only where they

can be distinguished from the data. This requires an artefact to have an uncharacteristic frequency or orientation. Although directional frequency components can exist within the landscape (for example a dominant valley or a geologically controlled drainage systems) and consequently be apparent in the frequency domain, such features were not present in the two study area datasets. However, high frequency diagonal components were apparent in the FFT frequency data, their orientation orthogonal to that of the diagonal artefacts within both study areas. In both cases these formed distinctive and clear components of the FFT frequency data. Unlike spatial filtering, filtering in the spectral domain can be and was applied to specific frequencies within a dataset, minimizing data smoothing and editing. Unwanted frequency components were removed by deleting them from the FFT frequency data with a user defined polygon layer that delineated the boundary between artefact and data within the frequency domain. This was subsequently used as a cut filter, essentially cutting the artefacts out of the dataset. This comprises the second stage of the spectral filtering. This identification and delineation of the error components is inherently subjective in those cases where the boundary between data and error is fuzzy and not crisp and should be performed only when the location of the anomalous frequencies within the FFT data is clear.

An inverse transform was then performed transforming the data back into the spatial domain and reconstructing the missing cell values using their expected frequencies from within the modified FFT frequency data. This comprises the third and final stage of the spectral filtering. The procedure edits only the cells identified as error components (the frequencies removed from the FFT data), thereby limiting data smoothing and the introduction of further error. The resultant DEM is consequently comprised of the old DEM surface and the reconstructed elevation values for the elevation frequencies removed by the filter.

5. Results

Spectral filtering performance was assessed by comparison with the ability of mean smoothing filters to remove the frequency and spatial appearance of unwanted data artefacts and to minimize extensive data smoothing and editing. Although validation elevation data were not available, filter performance was assessed through examination of frequency distributions, elevation modifications, resultant topography and structure of surface derivatives and extracted flow networks.

5.1. Norwegian 100 m elevation model

Spatial filters. Low-pass filters with a 3×3 , 5×5 , 7×7 and 9×9 kernel window were applied to the DEM. All of the low-pass filters smoothed the data and muted diagonal trends and spikes (Figure 2b), but failed to remove artefacts following two consecutive applications (Figure 5a). Although failing to remove artefacts, these filters made considerable changes to the distribution of values within the DEM, altering the data distribution by reducing the data range and standard deviation (Table I). Increasing smoothing was observed as filter size and number of applications increased. Elevation maxima and minima, predominantly located along ridge networks were subject to the largest changes of up to 380 m (Figure 5b). A single pass of the 3×3 filter edited >80% of cells by more than 1 m.

Examination of elevation changes produced by the filters highlights an increasing standard deviation with filter size and repetition (Table II). The nature of the mean filters resulted in very little difference to the mean elevation value within each output DEM. Further evidence of the ability of the mean filters to remove error is evident through examination of resultant DEM frequency histograms, these displayed a smoother distribution with size and application of the filters. The spatial distribution of elevation changes showed the global smoothing performed by the filters, with larger changes occurring on key landscape components: peaks and ridges (Figure 5b).

Discussion of the extracted flow network is necessarily speculative, as in part these reflect the inadequacies of the extraction algorithm and data resolution. Alterations to the extracted network from a single pass of the 3×3 filter were minimal and all parallel and linear flow segments remain (Figure 3b). Extracted flow networks for coarser filters were not tested, because data resolution was degraded and scale effects in landform definition (Wood, 1996; Arrell et al., 2007) and network extraction would complicate interpretation.

Spectral filtering. Diagonal components within the FFT frequency data were identified as representing the striped DEM artefacts, and had a repetitive and asymmetric structure. Their soft boundaries and vague extent suggest that they are present at a range of elevation frequencies, yet not systematic throughout the DEM (Figure 6).

The spectral filtering muted diagonal trends and contour altitude peaks within the Norwegian DEM (Figures 2c and 5c,d). Examination of the distribution of elevation values within the output DEM identifies the spectral filter as a less severe filter than the mean filters, where minimal changes were made to the range and distribution of data values (Tables I and II). Further evidence of the intensity of smoothing performed by the spectral filter is visible in altitudinal changes produced by the filter. The mean alteration to elevation values is 0 m and the maximum and minimum are 66 m and -69 m, respectively. These values are nearly an order of magnitude less than the equivalent spatial filtering changes (Table II), and less than 50% of cells were altered by more than 1 m.

The spatial structure of these changes also provided evidence of the minimal disruption of the spectral filtering. Unlike the mean filtering approaches, altitudinal adjustments were largely restricted to the diagonal structure of the DEM error (Figure 5d). A comparative examination of changes from the spatial filtering highlighted more invasive data editing with data throughout the DEM being smoothed (Figure 5b).

Comparison of the frequency distributions of the original and filtered DEM did show some changes in data distribution. Most notable are small alterations to highest and lowest altitudes (Table II). The resultant frequency histogram had a much less erratic distribution and showed removal of most spikes (Figure 2c). Although every attempt was made to reduce the smoothing effect of the error removal procedure, some smoothing did occur. Removing high frequency components from the FFT data will in some cases remove high frequency landform components, where a soft boundary between noise and data makes discrimination difficult. However, in this application data edits were predominantly constrained to spatially and spectrally organized data artefacts (Figure 5d).

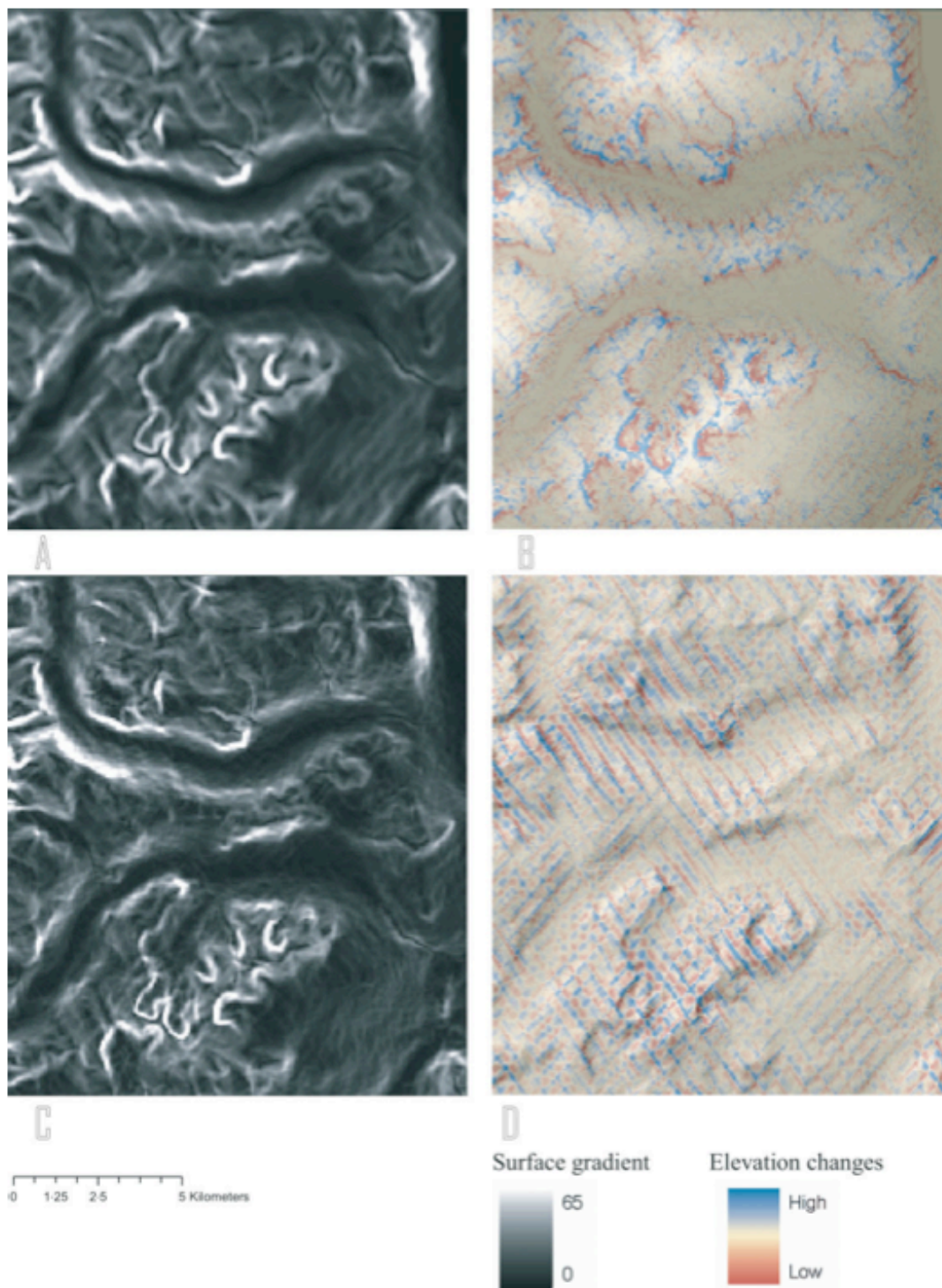


Figure 5. Subsection of Norwegian 100 m digital elevation model (DEM) showing: (A) surface gradient and (B) elevation differences between original and resultant DEM for a single pass of the 3×3 smoothing filter; (C) surface gradient and (D) elevation differences for spectrally filtered DEM. Within the 3×3 data, diagonal artefacts still remain in the surface gradient data and largest changes in elevations were made on peaks and ridges. In contrast the spectrally filtered data show that diagonal artefacts have largely been removed from the surface gradient data and elevation changes made by the filter shown in (D) are largely restricted to areas with dominant artefacts, global data smoothing has not been performed and largest changes do not occur on peaks and ridges as found in the equivalent 3×3 spatial mean filter dataset shown in (B). DEM copyright Statens kartverk.

Table I. DEM descriptive statistics for original and resultant 100 m Norwegian DEMs for the different size and repetition of spatial mean and FFT filters. Increasing size and application of filters leads to trends in the standard deviation and range of elevation data. FFT data maintain the range and standard deviation of the original data.

Filter	Minimum (m)	Maximum (m)	Mean (m)	Standard deviation
Original DEM	480	2472	1440	318
3 * 3	480	2426	1439	316
3 * 3 twice	487	2396	1439	315
5 * 5	494	2381	1439	314
5 * 5 twice	507	2359	1439	311
7 * 7	506	2355	1439	311
7 * 7 twice	519	2320	1439	307
9 * 9	512	2325	1439	308
9 * 9 twice	538	2286	1439	302
FFT	459	2454	1440	317

Table II. Elevation changes made to the 100 m Norwegian DEM for the spatial and FFT DEMs, clear differences are apparent between the changes made by the spatial mean and FFT filters.

Filter	Minimum (m)	Maximum (m)	Mean (m)	Standard deviation
3 * 3	-318	160	1	12
3 * 3 twice	-321	172	1	15
5 * 5	-348	215	1	19
5 * 5 twice	-363	252	1	26
7 * 7	-370	266	1	28
7 * 7 twice	-382	307	1	38
9 * 9	-384	306	1	36
9 * 9 twice	-388	358	1	49
FFT	-66	69	0	9

Spectral filtering highlighted topographic patterns in the magnitude and distribution of digital elevation data artefacts. The ability of this method to delineate high intensity frequency components was improved in less complex terrain, where the artefact frequency was more consistent, reflecting the strong terrain dependence of DEM artefacts. Examination of changes in the distribution of gradients in initial and filtered DEMs indicated that steeper gradients were most susceptible to artefacts in the original surface. Spatial organization of removed data identified valley and slope sides as areas of most change. Comparison of the spatial autocorrelation (calculated with Moran's I and Geary's C) present in the initial and filtered DEMs indicated a reduction in spatial autocorrelation, thereby supporting a hypothesis that error was spatially autocorrelated (Table III).

The extracted drainage network from the spectrally filtered DEM represents a more realistic and less artefacted dataset than either the original or the spatially filtered DEM. Parallel flow segments present within the original DEM drainage flow network were removed, and few linear segments remained (Figure 3b).

Table III. Spatial autocorrelation statistics for the elevation datasets, before and after FFT application. Note the opposing trends in coefficients.

	Norway		Lake District	
	With Error	After Error Removal	With Error	After Error Removal
Moran's I	0.9955	0.9959	0.998800	0.998805
Geary's c	0.0045	0.0041	0.000173	0.000168

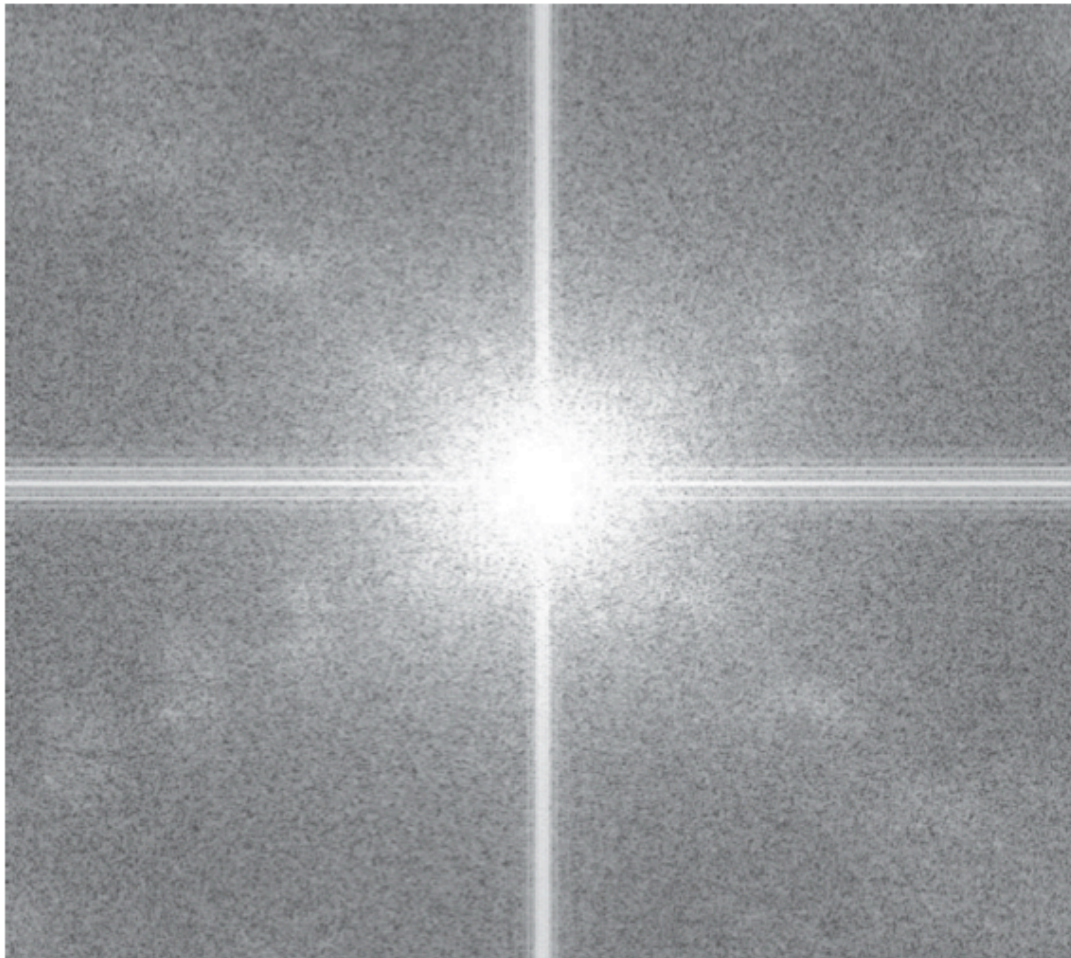


Figure 6. FFT frequency data for the 100 m Norwegian DEM, note the strong crosshairs and the diagonal banding representing the data artefacts.

5.2. Lake District 2 m DEM

Spatial filters. Low-pass filters with a 3×3 , 5×5 , 7×7 and 9×9 kernel window were applied to the DSM. Again, all these filters smoothed the data (Figure 7a and Table IV) and made large alterations to the original surface (Table V), but only repeat cycles or the 7×7 or 9×9 filters removed data artefacts (Figure 7a).

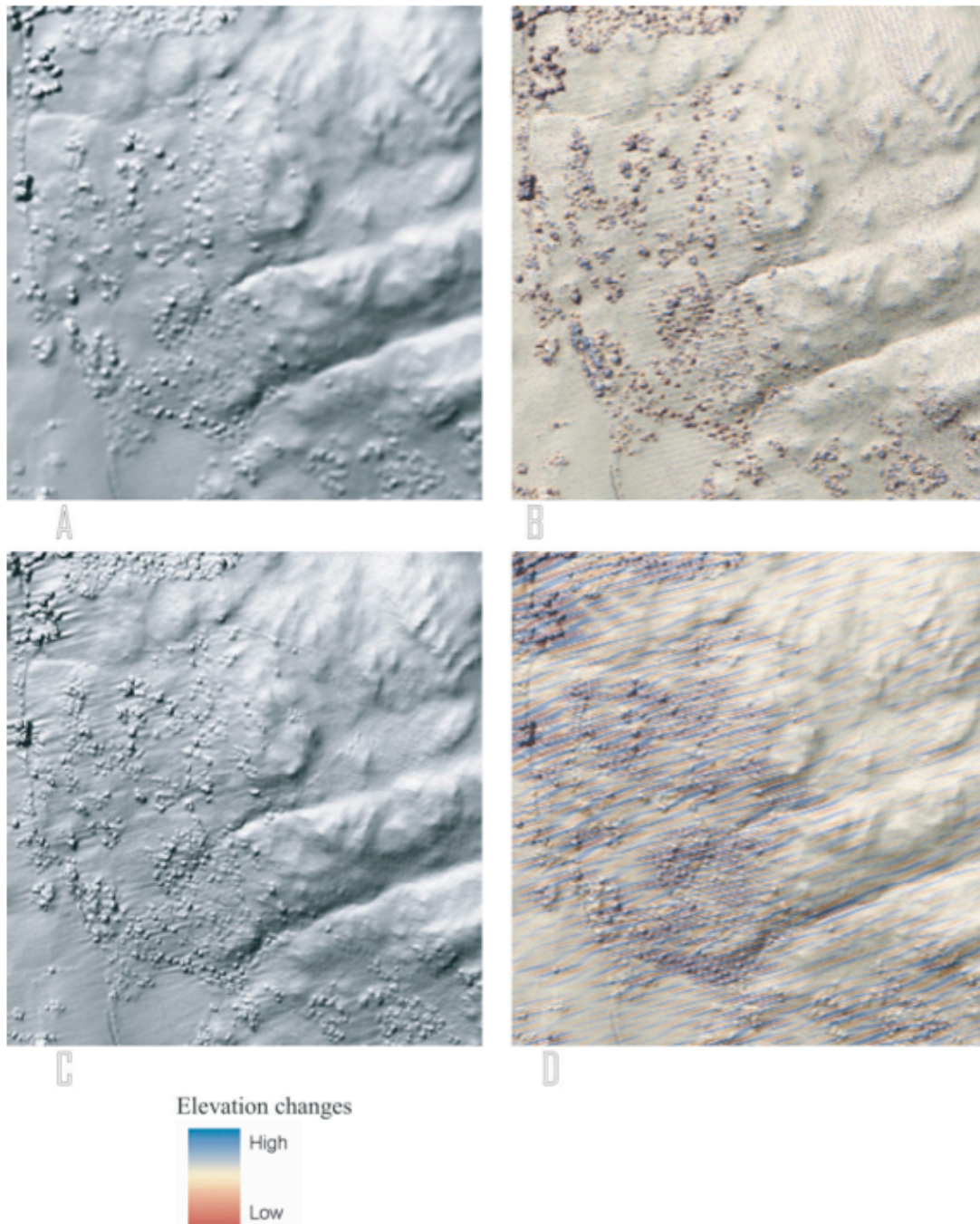


Figure 7. Subset of the LiDAR DSM a) hillshade image of the 3*3 processed data b) elevation differences made by the 3*3 filter. The hillshade image shows that most of the artefacts have been removed, but also shows a much smoothed surface, areas of largest elevation changes b) were made around the trees on the west of the dataset. Equivalent data for the FFT data are shown in c) hillshade data and d) elevation differences between the original and FFT DSM. Although the diagonal artefacts have been removed, other surface features have been introduced to the data, most noticeably surrounding the woodland area. Largest elevation changes were made in areas where artefacts were most apparent in the original dataset.

All mean filters smoothed the DSM elevation frequency distribution and reduced data range and standard deviation. A single pass of a 3×3 filter made elevation changes of up to 29 m, yet 98.5% of cells had their elevation changed by less than 1 m (Table V). An interesting trend within the smoothed data is the maximum reduction of altitudes as filter size and applications increased. This is likely to represent the increasing role

of locally high altitudes as filter neighbourhood size increases. This trend was not observed in Norway, which had a higher and rougher relief and where elevation values had a normal distribution. This may reflect the frequency distribution of the LiDAR data, which is positively skewed and platykurtic, suggesting that smoothing data through averaging is not the most appropriate technique when data do not conform to a normal distribution.

Table IV. DSM descriptive statistics for original and resultant 2 m LiDAR DSM for the different size and repetition of spatial mean and FFT filters. Increasing size and application of filters lead to trends in the standard deviation and range of elevation data. FFT data maintain the range and standard deviation of the original data.

Filter	Minimum (m)	Maximum (m)	Mean (m)	Standard deviation
Original DEM	90.40	335.04	208.73	64.47
3 * 3	90.89	334.93	208.73	64.46
3 * 3 twice	91.31	334.86	208.73	64.45
5 * 5	91.51	334.79	208.73	64.45
5 * 5 twice	92.19	334.48	208.73	64.44
7 * 7	92.03	334.52	208.73	64.44
7 * 7 twice	92.96	333.88	208.73	64.42
9 * 9	92.53	334.07	208.73	64.42
9 * 9 twice	93.69	333.25	208.74	64.39
FFT	90.45	335.08	208.73	64.47

Table V. Elevation changes made to the 2 m LiDAR DSM for the spatial and FFT DEMs, clear differences are apparent between the changes made by the spatial mean and FFT filters.

Filter	Minimum (m)	Maximum (m)	Mean (m)	Standard deviation
3 * 3	-21.82	29.01	0	0.67
3 * 3 twice	-17.96	29.68	0	0.70
5 * 5	-17.61	32.32	0.001	0.81
5 * 5 twice	-12.01	32.48	0.001	0.81
7 * 7	-11.77	33.51	0.002	0.91
7 * 7 twice	-8.48	33.37	0.003	1.00
9 * 9	-9.46	33.61	0.004	1.00
9 * 9 twice	-6.88	33.88	0.006	1.12
FFT	-3.85	4.11	0	0.21

Examination of the spatial distribution of elevation changes highlighted that most change occurred within forested areas, with local altitude changes being strongly influenced by tree height with local reductions in elevations at the edge of the canopy and local increases in elevations in the middle of the canopy (Figure 7b).

Propagation of data artefacts was explored in flow direction and extracted hydrological network data from a single pass of a 3×3 mean filter. The filter did mute diagonal artefacts in flow direction data but was unable to remove them. The filtered DSM introduced parallel and linear stream segments where local surface heterogeneity was reduced (Figure 8).

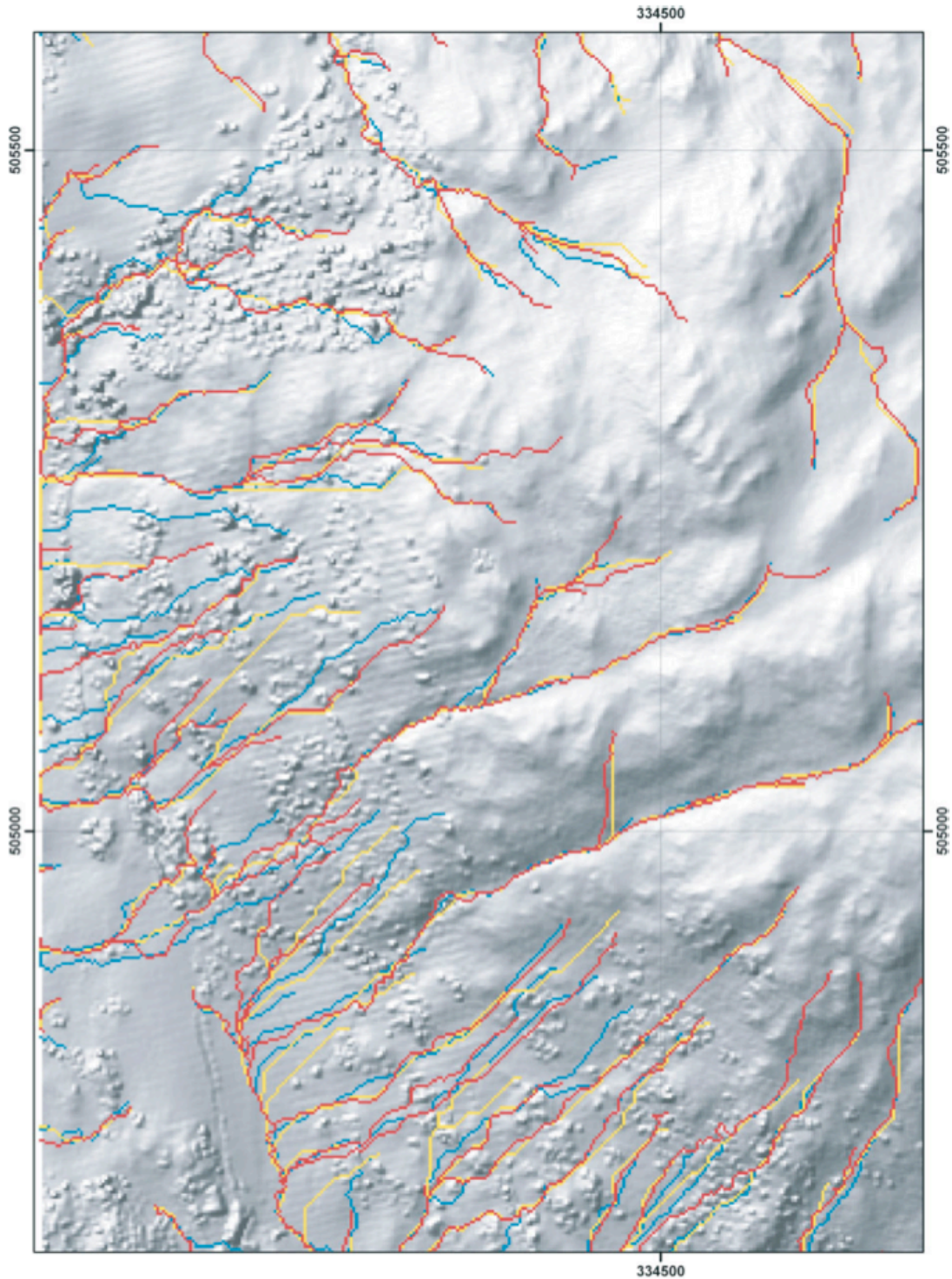


Figure 8. Flow accumulation networks draped on the hillshaded original DSM for the original (red lines), 3*3 filtered (yellow lines) and FFT filtered (blue lines) DSM for the Loughrigg data set. The 3 * 3 filtered DSM network shows multiple linear flow segments, which are not present in the original or FFT networks.

The spatial filters were more effective at removing artefacts present in the Loughrigg data than the Norwegian dataset. However, mean filter limitations were still apparent, making large alterations to data distribution and range, reducing data resolution and precision.

Spectral filtering. The FFT frequency data contained two components that were identified to have an orientation reflecting that of the data artefacts (Figure 9). Removing these components from the frequency data, reduced artefact magnitude in some areas of the study area, most noticeably within forested areas, but its effectiveness was not uniform throughout the DSM (Figure 7c). Alterations to elevation values were small (maximum 4.1 m) and again were nearly an order of magnitude less than those imposed by the spatial filters, with minimal differences made to data range and distribution (Figure 7d and Tables IV and V) and only 0.1% of cells were changed by more than 1 m.

Examination of the spatial distribution of these elevation changes showed that artefact removal was most effective within forested areas of the study area. Elevation changes exhibited a strong NNE and SSW orientation, matching that of one set of data artefacts (Figures 4 and 7c). Although the spectral filtering performed well at identifying and removing these artefacts, it did not identify artefacts with a NNW–SSE orientation. This reflects the relative magnitude of both artefact components, where the more dominant NNE and SSW orientations were distinctive within the frequency domain, and were consequently identified and removed. Lower magnitude NNW–SSE artefacts could not be differentiated within the frequency domain and consequently remain in the data.

Comparison of data spatial autocorrelation before and after the spectral filtering showed a slight increase, which suggests either that artefacts reduced the natural spatial autocorrelation in the landscape, or that the inverse transform itself introduced artefacts that increased the data spatial autocorrelation (Table III). The latter is the more likely, as unlike the Norwegian dataset, the resultant DSM contained surface elements that were not present within the original data, suggesting that the data artefacts were not accurately delineated within the FFT frequency data.

Implications for artefact propagation were again explored using surface slope, flow direction and flow accumulation networks. Striped artefacts were less well defined in the FFT modified flow direction data than in the original or the spatially filtered data. This improvement in appearance of flow direction data will minimize error propagation from striped artefacts in any subsequent analysis. The extracted flow network from the resultant DSM is very similar to the original network and contains no parallel or linear flow segments (Figure 8).

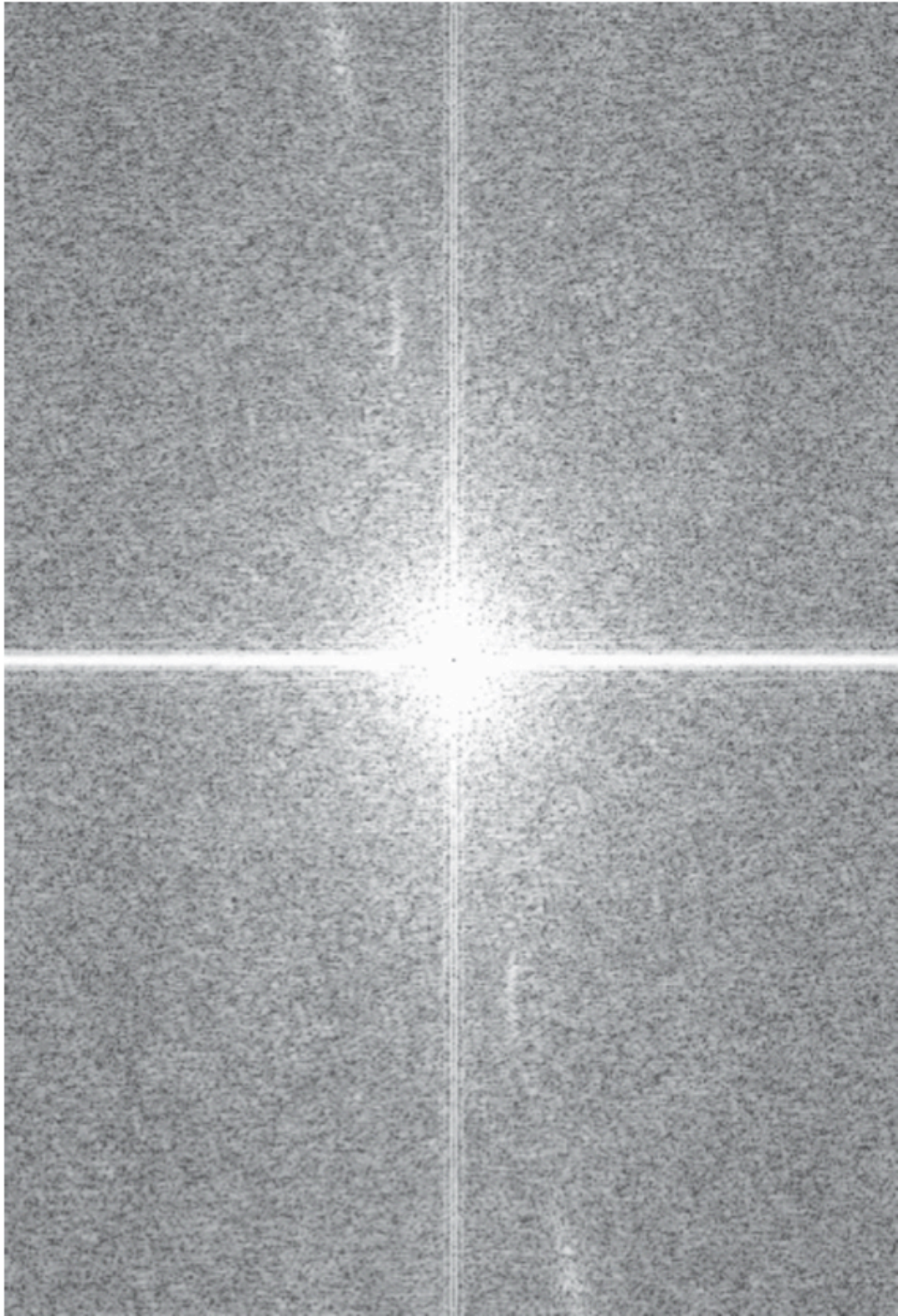


Figure 9. FFT frequency data of the 2 m LiDAR DEM showing strong crosshairs and diagonal high frequency components.

6. Discussion

Traditional spatial mean filters and spectral filtering were compared in order to assess their ability to discriminate between signal and error within two striped digital elevation datasets.

The application of spectral filtering showed marked improvements in artefact removal where the magnitude of artefact error is distinguishable in the Fourier frequency data. This is apparent in the Norwegian DEM, where artefacts form a dominant component of the FFT frequency dataset. Here spectral filtering showed considerable advantages over traditional mean filtering techniques, where data edits were restricted to artefact frequencies (Figure 5d). We propose that under these conditions, and after examination of the FFT data, artefacts should be removed and delineated using spectral filtering over traditional smoothing filters, where loss of precision and variance within original data is minimized.

Where an error component is not distinguishable from other low or high frequency data, application of spectral filtering does not perform as effectively and may not be appropriate. This is apparent through examination of the 2 m LiDAR DSM, although diagonal artefacts are present in the data they were not entirely distinguishable within the frequency domain. Spatial filtering also failed to remove these artefacts, while maintaining reasonable data resolution (Figure 7a). Even though performance of the spectral filtering in the LiDAR case study may appear disappointing it simply reflects complexities of signal processing, where unless signal and error can be differentiated, error alone cannot be removed. Under these conditions spatial mean smoothing may be appropriate and is proposed by some researchers as a method of incorporating data variance where errors are hidden within data variability. Spatial filtering is less appropriate in a case where local artefact or error magnitude is large. Here, erroneous elevation values will bias any mean calculations, where artificially high or low values will compromise mean averaging. In such cases spectral filtering would be more appropriate where these large magnitude data values can be removed from the dataset.

It should be noted that the size and scale of the sample DEM controls the relative frequencies of any error components, where small frequency artefacts are unlikely to be distinguishable with a large and varied topography where data and artefact frequency is matched with natural variability in the land surface. However, within a smaller and smoother topography their relative magnitude will be greater, and consequently more likely to be visible within the frequency domain. Many traditional filters also perform less effectively in complex terrain. However, the spectral filtering still performs well, when artefact frequency is persistent throughout a DEM. Unlike traditional filtering techniques, spectral filtering does not attempt to identify or remove error within a local neighbourhood, but simply represents the distribution of frequencies present within the data. Spatially or frequency persistent artefacts will be evident in the FFT data. This was apparent in the study results, where in the Norwegian DEM, the relative magnitude and frequency of data artefacts were large enough to distinguish them from the natural variability within the data. In contrast, within the Lake District DSM only in some areas was such delineation possible.

The results presented here suggest that DEM artefact or error removal using spectral filtering is more advantageous than mean spatial filters for geomorphological applications when maintaining topographic structures and data range and standard deviation is important. Traditional mean spatial filters make considerable changes to

the morphometric characteristics of a landsurface, lowering peaks, smoothing ridges and raising valleys. These changes will clearly have implications for any subsequent DEM applications where the shape and nature of the terrain surface is considered. Although spectral filtering also alters the terrain surface, modifications to the distribution and structure of elevation values are minimal and made using information on the spatial and frequency characteristics of the original elevation data. Results also indicate that the inverse FFT better estimates replacement data values than mean filters; indicated through improvements to extracted flow networks, where spectrally filtered DEMs remove and do not introduce linear or parallel flow paths. Comparative results from the mean filters showed that despite substantial modifications to the elevation dataset, inadequacies in the flow network data remained.

Limitations in the application of spectral filters still exist, primarily the delineation of artefact or error components within the FFT frequency data. Unlike traditional filtering techniques where data editing is automated, this is the most critical stage of the filtering and the least automated. Examination of frequency histograms of FFT frequency data provides opportunities for future work to automate delineation of uncharacteristic frequency components, using exact frequency ranges.

7. Conclusions

Spatial mean filters were shown to make large alterations to the distribution and range of elevations within the study DEM and DSM, which raises several issues about their suitability for digital elevation data processing. Although a range of spatial filters were applied to the two datasets none were found to be capable of identifying and removing artefacts within the digital elevation data effectively.

Spectral filtering identified the implicit spatial and explicit spectral characteristics of the striped artefacts present within the digital elevation data. The technique avoided global smoothing and simply altered data identified as uncharacteristic. However, care is encouraged when differentiating between high frequency landscape components and high frequency data artefacts.

The technique presented here is considered to provide an effective mechanism for visualizing and removing spatially and spectrally organized digital elevation artefacts, such as the striped artefacts shown here, and may be of particular relevance in the processing of LiDAR data. Future work will explore the appropriateness of the technique for different data resolutions, error types and different surface complexities. We will also explore the use of data windowing to identify and remove any aliasing effects present when analysing large datasets.

The use of spectral filtering to remove striped data artefacts has been shown to provide considerable advantages over traditional spatial filters for DEM applications where data artefacts are distinguishable from data in the frequency domain, particularly those interested in the structure and form of the land surface. Spectral filtering makes minimal alterations to the distribution and structure of the terrain surface, preventing loss of data precision and variability.

8. References

- Aguilar F, Aguilar M, Agüera F, Sánchez J. 2006. The accuracy of grid digital elevation models linearly constructed from scattered sample data. *International Journal of Geographical Information Science* **20**: 169-192.
- Albani M, Klinkenberg B. 2003. A spatial filter for removal of striping artifacts in digital elevation models. *Photogrammetric Engineering and Remote Sensing* **69**: 755-765.
- Arnold N, Rees W, Devereux B, Amable G. 2006. Evaluating the potential of high-resolution airborne LiDAR data in glaciology. *International Journal of Remote Sensing* **27**: 1233-1251.
- Arrell K. 2005. *Predicting Glacier Accumulation Area Distributions*. Unpublished PhD. Thesis. Durham University, Durham, UK.
- Arrell K, Fisher P, Tate N. In press. A fuzzy *k*-means classification of the natural landforms in Snowdonia, Wales. *Computers and Geosciences*.
- Baltsavias E. 1999. A comparison between photogrammetry and laser scanning. *ISPRS Journal of Photogrammetry and Remote Sensing* **54**: 83-94.
- Brandtberg T. 2007. Classifying individual tree species under leaf-off and leaf-on conditions using airborne LiDAR. *ISPRS Journal of Photogrammetry and Remote Sensing* **61**: 325-340.
- Brown DG, Bara TJ. 1994. Recognition and reduction of systematic error in elevation and derivative surface from 7 1/2 -minute DEMs. *Photogrammetric Engineering and Remote Sensing* **60**: 189-194.
- Brunson EG, Olsen RW. 1978. Data digital elevation model collection systems. *Proceedings of the digital terrain models (DTM) Symposium*, 9-11 May, St. Louis, Missouri (American Society of Photogrammetry, Falls Church, Virginia), pp 72-99.
- Champeney D. 1973. *Fourier transforms and their physical applications*. London: Academic Press, 256pp.
- Chen Q. 2007. Airborne LiDAR data extraction and information processing. *Photogrammetric Engineering and Remote Sensing* **73**: 109-112
- Christensen AH. 1987. Fitting a triangulation to contour lines. In *Proceedings Auto Carto 8*. ASPRS/ACSM, Falls Church, Virginia.
- Cooper MAR. 1998. Datums, Coordinates and Differences. In *Landform Monitoring, Modelling and Analysis*, Lane SN, Richards KS, Chandler JH (eds) J. Wiley and Sons, Chichester.

- Crutchley S. 2006. Light detection and ranging (LiDAR) in the Witham Valley, Lincolnshire: an assessment of remote sensing techniques. *Archaeological Prospection* **13**: 251-257.
- Dobrin M, Ingalls, A, Long J. 1965. Velocity and frequency filtering of seismic data using laser light. *Geophysics* **30**: 1144-1178.
- Eichinger W, Cooper D. 2007. Using LiDAR remote sensing for spatially resolved measurements of evaporation and other meteorological parameters. *Agronomy Journal* **99**: 255-271.
- Felicitimo AM. 1994. Parametric Statistical-Method for Error-Detection in Digital Elevation Models. *ISPRS Journal of Photogrammetry and Remote Sensing* **49**: 29-33.
- Fisher PF, Tate NJ. 2006. Causes and consequences of error in digital elevation models. *Progress in Physical Geography* **30**: 467-489.
- Fisher PF. 1998. Improved Modeling of Elevation Error with Geostatistics. *Geoinformatica* **2**: 215-233.
- Hannah MJ. 1981. Error-Detection and Correction in Digital Terrain Models. *Photogrammetric Engineering and Remote Sensing* **47**: 63-69.
- Hassan, 1988
- Hengl T, Evans I. 2007. Geomorphometry: a brief guide. In *Geomorphometry: concepts, software, applications*, Hengl T, Reuter HI. (eds) Office for Official Publications of the European Communities.
- Holmes K, Chadwick O, Kyriakidis P. 2000. Error in a USGS 30-meter digital elevation model and its impact on terrain modeling. *Journal of Hydrology* **233**: 154-173.
- Hunter GJ, Goodchild MF. 1997. Modeling the uncertainty of slope and aspect estimates derived from spatial databases. *Geographical Analysis* **29**: 35-49.
- Hutchinson MF. 1989. A New Procedure for Gridding Elevation and Stream Line Data with Automatic Removal of Spurious Pits. *Journal of Hydrology* **106**: 211-232.
- Flood M. 2001. LiDAR activities and research priorities in the commercial sector. *IAPRS*. Annapolis, MD, 22-24 Oct. 2001, 678-684.
- Florinsky I. 1998. Accuracy of local topographic variables derived from digital elevation models. *International Journal of Geographical Information Science* **12**: 47-62.
- Garbrecht J, Starks P. 1995. Note on the use of USGS Level 1 7.5-Minute DEM coverages for landscape drainage analysis. *Photogrammetric Engineering and Remote Sensing* **61**: 519-522.

Guth PL. 1992. Contour line ghosts in USGS level 2 DEMs. *Photogrammetric Engineering and Remote Sensing* **65**: 289-297.

James T, Barr S, Lane S. 2006. Automated correction of surface obstruction errors in digital surface models using off-the-shelf image processing. *The Photogrammetric Record* **21**: 373-397.

Jenson SK, Domingue JO. 1988. Extracting Topographic Structure from Digital Elevation Data for Geographic Information-System Analysis. *Photogrammetric Engineering and Remote Sensing* **54**: 1593-1600.

Klinkenberg B, Goodchild MF. 1992. The fractal properties of topography: A comparison of Methods. *Earth Surface Processes and Landforms* **17**: 217-234.

Kok A, Rangayyan RM. 1987. Filtering of digitally correlated Gestalt elevation data. *Photogrammetric Engineering and Remote Sensing* **53**: 535-538.

Kumler MP. 1994. An intensive comparison of Triangulated Irregular Networks (TINs) and Digital Elevation Models (DEMs). *Cartographica* **31**: 1-99.

Li Z. 1994. A comparative study of the accuracy of digital terrain models (DTMs) based on various data models. *International Journal of Photogrammetry and Remote Sensing* **49**, 2-11.

Lindsay J. 2006. Sensitivity of channel mapping techniques to uncertainty in digital elevation data. *International Journal of Geographical Information Science* **20**: 669-692.

Little JJ, Shi P. 2001. Structural lines, TINs, and DEMs. *Algorithmica* **30**: 243-263.

Liu H, Jezek K. 1999. Investigating DEM error patterns by directional variograms and Fourier analysis. *Geographical Analysis* **31**: 249-266.

Lloyd C, Atkinson P. 2006. Deriving ground surface digital elevation models from LiDAR data with geostatistics. *International Journal of Geographical Information Science*. **20**: 535-563.

Ma R. 2005. DEM generation and building detection from LiDAR data. *Photogrammetric Engineering and Remote Sensing* **71**: 847-854.

Monckton CG. 1994. An investigation into the spatial structure of error in digital elevation data. In *Innovations in GIS I*, Worboys MF. (ed). London, Taylor and Francis; 201-211.

Oksanen J, Sarjakoski T. 2006. Uncovering the statistical and spatial characteristics of fine topocscale DEM error. *International Journal of Geographical Information Science* **20**: 345-369.

Oimoen MJ. 2000. An effective filter for removal of production artefacts in U.S. Geological Survey 7.5-minute digital elevation models, *Proceedings of the Fourteenth*

International Conference on Applied Geologic Remote Sensing. 06–08 November, Las Vegas, Nevada (Veridian ERIM International, Ann Arbor, Michigan), 311–319.

Peucker TK, Fowler RJ, Little JJ, Mark DM. 1978. The Triangulated Irregular Network. In *Proceedings, American Society of Photogrammetry, Digital Terrain Models Symposium*, St. Louis, Missouri, May 9-11, 1978. American Society of Photogrammetry, Falls Church, Virginia.

Raber G, Jenson J, Schill S, Schuckman K. 2002. Creation of digital terrain models using adaptive LiDAR vegetation point removal process. *Photogrammetric Engineering and Remote Sensing* **68**: 1307-1315.

Rayner JN. 1971. *An Introduction to Spectral Analysis. Monographs in spatial and environmental systems analysis*. Pion Limited, London.

Reutebuch S, McGaughey R, Andersen H, Carson W. 2003. Accuracy of a high resolution LiDAR terrain model under a conifer forest canopy. *Canadian Journal of Remote Sensing* **29**: 527-535.

Schulz W. 2007. Landslide susceptibility revealed by LiDAR imagery and historical records, Seattle, Washington. *Engineering Geology* **89**: 67-87.

Sithole G, Vosselman G. 2004. Experimental Comparison of Filter Algorithms for Bare Earth Extraction From Airborne Laser Scanning Point Clouds. *ISPRS Journal of Photogrammetry and Remote Sensing* **59**: 85-101.

Sithole G, Vosselman G. 2003 Comparison of filtering algorithms. *Workshop on 3-D reconstruction from airborne laser scanner and InSAR data*, October 8-10, 2003, Dresden, Germany Volume XXXIV Part 3/W13, ISSN 1682-1777, 71-78.

Su J, Bork E. 2006. Influence of vegetation, slope and LiDAR sampling angle on DEM accuracy. *Photogrammetric Engineering and Remote Sensing* **72**: 1265-1274.

Temme A, Heuvelink G, Schoorl J, Claessens L. 2007. Geostatistical simulation and error propagation in geomorphometry. In *Geomorphometry: concepts, software, applications*. Hengl T, Reuter HI. (eds) Office for Official Publications of the European Communities.

Thapa K, Bossler J. 1992. Accuracy of spatial data used in geographical information systems. *Photogrammetric Engineering and Remote Sensing* **58**. 835-841.

Walker W, Kelldorfer JM, Pierce L. 2007. Quality assessment of SRTM C- and X-band interferometric data: Implications for the retrieval of vegetation canopy height. *Remote Sensing of Environment* **106**: 428-448.

Wilson JP, Gallant JC. 2000. *Terrain Analysis*. John Wiley and Son, New York, 303pp.

Wise SM. 1998. The effect of GIS interpolation errors on the use of DEMs in geomorphology. In *Landform Monitoring, Modeling and Analysis*. Lane SN, Richards KS, Chandler JH. (eds) John Wiley and Sons, Chichester.

Wise SM. 2002. *GIS Basics*. Taylor and Francis, London, 218pp.

Wise SM. 2000. Assessing the quality for hydrological applications of digital elevation models derived from contours. *Hydrological Processes* **14**: 1909-1929.

Wood J. 1986. *The Geomorphological Characterisation of Digital Elevation Models*, Unpublished PhD. Thesis, University of Leicester, UK.

Wood JD, Fisher PF. 1993. Assessing interpolation accuracy in elevation models. *IEEE Comp. Graphics and Applications* **13**: 48-56.